**Advances in Concrete Construction,** *Vol. 22, No. 1 (2026) 53-73*
https://doi.org/10.12989/acc.2026.22.1.053

Techno-Press

# Investigation of shear behavior in geopolymer concrete beams with different ratios of slag and polyamide fibers under oven and ambient curing condition

Ali İhsan Çelik[1], Ufuk Tunç[1], Memduh Karalar[2], Atahan Güven[1], Yasin Onuralp Özkılıç*[3,4,5]

[1]*Department of Construction, Tomarza Mustafa Akincioglu Vocational School, Kayseri University, Kayseri, 38940, Turkey*
[2]*Department of Civil Engineering, Zonguldak Bulent Ecevit University, Zonguldak, Turkey*
[3]*Department of Civil Engineering, Faculty of Engineering, Necmettin Erbakan University, Konya 42000, Turkey*
[4]*Department of Unique Buildings and Constructions Engineering, Don State Technical University, Gagarin Sq. 1, 344003 Rostov-on-Don, Russia*
[5]*Department of Technical Sciences, Western Caspian University, Baku, 1001, Azerbaijan*

*(Received November 2, 2025, Revised June 3, 2026, Accepted June 4, 2026)*

**Abstract.** The purpose of this study was to investigate the effect that varying proportions of slag and polyamide fibers have on the shear performance of reinforcing geopolymer concrete. For the purpose of accomplishing this goal, the performance of geopolymer concrete was evaluated by adjusting the ratios of slag to polyamide fiber and the percentage of replacement. Furthermore, it was investigated how to reinforce geopolymer concrete by combining ambient and oven curing techniques. The slag ratio was adjusted in various amounts, such as 5%, 10%, and 15%, to accomplish this aim. The polyamide fiber ratios, however, were determined to be 1%, 2%, and 3%, respectively. This aim was attained by creating a total of twelve distinct mixing proportion examples. The impact of altering the slag ratio while maintaining a constant polypropylene fiber ratio was examined in this study. When the slag ratio was increased by 15%, the load bearing capacities of R-C-Bs were directly improved by 21.85% and 10.28%, respectively, when they were cured in an oven and in an ambient environment. Furthermore, it was found that by increasing the ratio of polypropylene fibers by 1% during the ambient and oven curing processes, the load carrying capacity of R-C-B was significantly increased by 10.59% and 3.61%, respectively. The findings of the research demonstrated that the use of an oven curing technique to the concrete resulted in a considerable improvement in the reinforcing geopolymer concrete's ability to be strengthened. Furthermore, the experimental results obtained were compared with various design codes, including ACI-318, CEB-FIB, Eurocode, and the Iranian National Building Codes.

**Keywords:** ambient curing; oven curing; polyamide fibers; reinforcement geopolymer concrete; shear behavior; slag ratio

## 1. Introduction

In the last several decades, research has been conducted on geopolymer concrete (GPC), a

*Corresponding author, Associate Professor, E-mail: yozkilic@erbakan.edu.tr

**Copyright © 2026 Techno-Press**

ISSN: 2287-5301 (Print), 2287-531X (Online)

potential sustainable building material that uses industrial byproducts to reduce CO2 emissions. With its innovative, affordable, and environmentally friendly components, geopolymer-based concrete is a perfect combination that has all the necessary qualities to replace traditional cement [1, 2]. Inorganic aluminosilicates, or geo-polymer materials, are created by combining alkaline solutions with silica and aluminum-rich source materials [3]. So, after combining the sodium silicate and sodium hydroxide solutions to create an alkaline activated solution, waste materials like fly ash (FA) are used to create GPC [3]. In recent years, there has been a trend of partly substituting Ordinary Portland Cement with fly ash waste material in the production of concrete [4]. An impressive achievement has been made in the creation of high-volume fly ash concrete, where up to 60% of ordinary Portland cement has been replaced by fly ash. Despite this substitution, the concrete nevertheless has exceptional technical qualities and demonstrates excellent durability performance [5-8]. When considering environmentally friendly materials and sustainable growth in the construction sector, GPC shows great promise as an Ordinary Portland Cement substitute. Additionally, when the appropriate mix design is used, GPC may exhibit better mechanical and chemical qualities in comparison to traditional concrete [9-14]. Because of all these earlier benefits, geopolymers appear promise as construction materials. Numerous studies have been conducted in relation to the creation of geopolymer concrete in order to comprehend the mechanical attributes, fire resistance, and strength characteristics of GPC [15, 16]. In the literature, there have been several efforts to cure geopolymer under ambient conditions. [17] presented the results of an experiment on physical and mechanical characteristics that of geopolymer concrete. For this purpose, Geopolymer concrete based on fly ash was the subject of the experiments, and several curing methods were used. According to the results of the compressive strength test, specimens that were cured in an ambient environment demonstrated a significant increase in compressive strength with curing age. However, specimens that were cured in an oven showed a negligible change in strength with curing age when compared to specimens that were cured in an ambient environment [17]. While fly ash and slag were mixed together to create geopolymer concrete, [18] found that this had an impact on the concrete's setting a period of time functionality, and initial strength behavior while it cured in an ambient environment. The results were comparable to those of Ordinary Portland Cement concrete. Research revealed that the addition of GGBS resulted in the generation of internal heat within the mixture. This heat facilitated the geopolymerisation process during ambient curing and led to significant early strength growth [19-21]. In another study performed was Perera et al. [22]. This research found that curing metakaolin-based geopolymers at room temperature resulted in a significant increase in strength, comparable to that achieved by oven curing. However, the strength of specimens treated at high temperatures increased fast within a day. In a different study, Heah et al. [23] found that ambient curing metakaolin-based geopolymers results in much lower strength than oven curing. In order to examine the impact of curing temperatures (10, 20, 40, 60, and 80°C) and times on the microstructure, pore distribution, and compressive and flexural strengths of alkali-activated metakaolin material, Rovnanik [24] conducted research. Mechanical experiments that were evaluated revealed that the curing temperature had a significant impact on the mechanical characteristics of the geopolymer material, both at an early age and in its final stages. Elevated curing temperatures enhance the compressive and flexural strengths during the first stages, potentially achieving the desired values within a span of 24 hours. Shoaei et al. [25] examined how different amounts of natural zeolite affected the characteristics of geopolymer mortars. These mortars were activated with sodium metasilicate and tested under various curing settings to assess their fresh and hardened qualities. The study revealed that the process of heat-curing significantly

enhances the mechanical strength of the mortars. The impact of heat processing on the cementitious functioning of Fly ash (FA) was examined by Wang et al. [26], who also identified the processes in cementitious materials. Fly ash cement's mechanical characteristics revealed the process of heat-activated FA reinforced cementitious materials. The findings indicate an increasing trend in the glass phase concentration of FA as the degrees of heat activation increases. Zheng et al. [27] noted how the mechanical and thermal characteristics, as well as the overall porosity, were affected by the sodium silicate solution concentration. For the synthesis of extremely porous geopolymers, the microwave foaming technique might be used as an effective and quick foaming approach. The assessment of an effective method for curing geopolymer concrete was investigated by Yewale and Nikam [28]. Sodium hydroxide and sodium silicate solutions were used to activate the class F fly ash used in the production of geopolymer concrete in the process. It was discovered via experimentation that the strength of the geopolymer concrete cubes increased with temperature, with 60℃ oven curing providing the highest strength. Kumaravel [29] performed another investigation. It was also proven that concrete conditioned in an oven had the optimal strength after a day at 60°C, but ambient-cured concrete had a significantly reduced compressive strength. Numerous investigations on the mechanical characteristics of geoplymer concrete in both oven and ambient settings have been conducted, as the aforementioned research demonstrate. In addition to these investigations, Many applications, including structural components, maritime structures, and the transportation sector, have made use of geopolymer concrete materials [30-32]. Some of the studies also utilized recycled and was materials into geopolymer [33-37]. Bernal et al. [38] examined the mechanical and flexibility characteristics of an alkali-activated slag concrete reinforced with steel fibers throughout its early stages of development. According to their findings, fiber-reinforced geopolymer concrete has superior mechanical characteristics compared to Portland cement concrete. The study conducted by Hassan et al. [39] focused on analyzing the structural performance of beams made of reinforced geopolymer concrete that incorporates steel fiber. In this experimental investigation, the reinforced geopolymer concrete beams were tested under four-point flexural stress conditions. The specimens' mid-span was used to measure the reinforced geopolymer concrete deflections. The results further demonstrate that the flexural strength and elastic modulus of reinforced geopolymer concrete were significantly improved as a result of the inclusion of steel fibers. Furthermore, the reinforced geopolymer concrete exhibited superior performance in flexural strength and other mechanical parameters compared to traditional concrete. Sumajouw and Rangan [40] performed another investigation. In this study, A total of twelve geopolymer concrete beams and twelve geopolymer concrete columns, which were reinforced, were produced and subjected to testing. Flexural behavior, including flexural strength, fracture pattern, deformation, and flexibility, of reinforced geopolymer concrete beams was reported. Relative to reinforced Portland cement concrete beams documented in studies, the fracture patterns discovered in reinforcement geopolymer concrete beams were comparable. Ferdous et al. [41] introduced a method for creating a mixture of fly-ash based geopolymer concrete and examined its use as filler material in a hybrid composite beam. Following that, an analysis is conducted to ascertain the potential use of geopolymer concrete filled hybrid composite beams in building structures by evaluating their structural performance. The behavior of the hybrid beam was evaluated by numerical and analytical methods, and the findings demonstrated a strong correlation with the experimental examination. Kumaravel and Thirugnanasambandam [42] performed another investigation. Flexible performance of GPC beams and cement concrete beams under control was studied by Kumaravel and Thirugnanasambandam [42]. Four beams in all are evaluated under static loads to failure across an effective span of 3000 mm. Theoretical findings

are compared with the load-displacement behavior of the geopolymer concrete beams and control beams. According to the findings, the flexural strength of the GPC beams was higher.The deflections of GPC beams are greater at various phases, including service load and peak load stages. Hutagi and Khadiranaikar [43] examined the bending properties of GPC beams cured at room temperature. Testing was performed on twelve reinforced concrete beams with dimensions of 175 millimeters by 250 millimeters by 1500 millimeters. When concrete ultimately crushed in the compression zone, a feature of the under-reinforced portions, all reinforced geopolymer concrete beams broke in a ductile manner in the flexure mode. Abdullah et al. [44] conducted a comparative analysis of the shear performance of reinforced ordinary Portland cement concrete beams and GPC beams with identical cross-sections and compressive strengths. In order to assess how concrete type and shear span affected the shear strength, the research evaluated nine beams under three-point bending. The findings indicated that, as the $a/d$ ratio increased, the shear strength drop rates for ordinary Portland cement concrete and GPC beams were comparatively comparable, but the failure mechanism changed from shear in ordinary Portland cement concrete beams to shear-flexure in GPC beams. As previously noted, only a small number of these research investigated the first GPC employing any type of reinforcement. Based on the information provided, it was noted that these studies concentrated on the advancement of sustainable GPC. Despite the fact that reinforced concrete beams containing GPC are a potentially useful building material, there aren't many research examining at their structural behavior. Therefore, the purpose of the present investigation is to examine the structural behavior of GPC beams reinforced by oven curing and ambient curing processes. Within the parameters of this investigation, the effects of various slag and polypropylene fiber proportions were examined. Consequently, the litterateur is provided with several significant supports through this investigation.

### 1.1 The significance of investigation

According to the previously indicated literature assessment, the few investigations on GPC mostly use oven curing techniques and ambient temperature. Nevertheless, there isn't any study on GPC that incorporates both slag and polypropylene fiber as components in the existing literature. One of the distinctive features of this research is that it studies GPC by using both slag and polypropylene fiber in its investigation. Although the flexural performance of GPC beams incorporating slag and polyamide fibers has been previously reported in [45], the corresponding shear behavior of similar beam configurations remains inadequately understood. The present study focuses specifically on the shear response of geopolymer concrete beams and examines the governing mechanisms of diagonal cracking, load transfer, and failure development under different material compositions and curing conditions. In this context, the role of slag content and polyamide fiber reinforcement is evaluated in terms of shear capacity, crack propagation, and deformation characteristics.

- To assess the shear performance of geopolimer concrete, the combined impact of numerous parameters, including polyamide fiber reinforcement and slag content, is taken into account.
- A novel viewpoint on the mechanical performance of geopolymer concretes is introduced by the hybrid curing approach (combined assessment of ambient and oven curing) used in this investigation.
- An innovative and application-oriented original contribution to the literature is provided by experimental analyses conducted on a total of 12 distinct mixture designs in comparison to

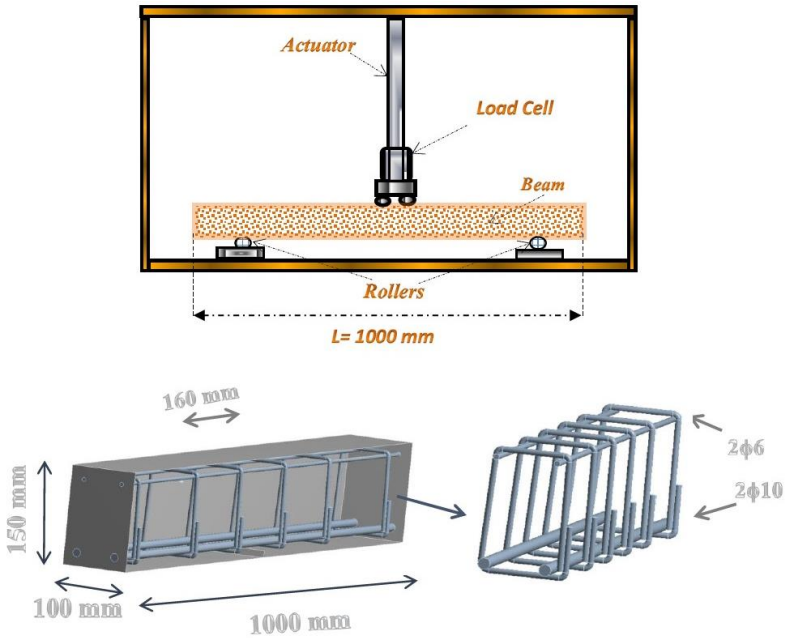



Figure 1. Arrangement for the test groups and display the arrangement of reinforcements for the specimens

international requirements.

Research results indicate that geopolymer, a material often used in concrete, is being utilized in a broader range of applications, including prestressed reinforced concrete beams. Further information is included in the following subsections.

## 2. Experimental procedure

The present investigation included the production of GPC using Polypropylene fibers and Slag. An investigation was conducted to analyze the impact of shear behavior on reinforcing GPC cured under ambient and oven conditions. There were a total of 12 distinct samples created with varying mixing ratios. The specimens were manufactured at Kayseri University. The experimental configuration of the specimens can be observed in Fig. 1. The examples were created to measure 1000 mm in length and 100×150 mm in cross-section. The test configuration described in Fig. 1 was used for four-point bending tests. The specimens were formulated taking into account five key parameters: polypropylene fiber, slag ratio, ambient conditions, oven curing, and stirrup spacing as given in Table 1. Various proportions of slag were changed, including 0%, 5%, 10%, and 15%, to achieve this goal. On the other hand, the proportions of Polypropylene fibers were chosen to be 1%, 2%, and 3%. There were one stirrup spacing used: 160 mm. Specifically, 2ϕ10 and 2ϕ6 were used as longitudinal reinforcement for the tension and compression zones According to the literature, RCBs will exhibit tensioned belt behavior if the a/d ratio is less than 2.5 [46]. The RCB behavior is more related to the shear behavior than bending since the a/d ratio of all the RCBs utilized in the trials was found to be 3.08. To enable a direct comparison of the effects of experimental variables, the cutting aperture/depth ratio (a/d) in this investigation was maintained

Table 1. GPC mix materials for 1 $m^3$

| | Sample no | Fly ash (kg) | SLAG (kg) | SLAG % | Polyamide Fiber (%) | Na2SiO3 (kg) | NaOH (kg) | Fine aggregate (kg) | Coarse aggregate (kg) |
|---|---|---|---|---|---|---|---|---|---|
| Ambinet | GPC1-A-S-1 | 380.16 | 20.00 | 5 | 0 | 171.43 | 68.57 | 633.49 | 1176.35 |
| | GPC2-A-S-2 | 360.13 | 40.01 | 10 | 0 | 171.43 | 68.57 | 633.50 | 1176.36 |
| | GPC3-A-S-3 | 340.13 | 60.02 | 15 | 0 | 171.43 | 68.57 | 633.50 | 1176.36 |
| | GPC4-A-S-4 | 380.16 | 20.00 | 10 | 1 | 171.43 | 68.57 | 633.49 | 1176.35 |
| | GPC5-A-S-5 | 360.13 | 40.01 | 10 | 2 | 171.43 | 68.57 | 633.50 | 1176.36 |
| | GPC6-A-S-6 | 340.13 | 60.02 | 10 | 3 | 171.43 | 68.57 | 633.50 | 1176.36 |
| Oven | GPC1-O-S-1 | 380.16 | 20.00 | 5 | 0 | 171.43 | 68.57 | 633.49 | 1176.35 |
| | GPC2-O-S-2 | 360.13 | 40.01 | 10 | 0 | 171.43 | 68.57 | 633.50 | 1176.36 |
| | GPC3-O-S-3 | 340.13 | 60.02 | 15 | 0 | 171.43 | 68.57 | 633.50 | 1176.36 |
| | GPC4-O-S-4 | 380.16 | 20.00 | 10 | 1 | 171.43 | 68.57 | 633.49 | 1176.35 |
| | GPC5-O-S-5 | 360.13 | 40.01 | 10 | 2 | 171.43 | 68.57 | 633.50 | 1176.36 |
| | GPC6-O-S-6 | 340.13 | 60.02 | 10 | 3 | 171.43 | 68.57 | 633.50 | 1176.36 |

constant in all samples. As a result, the impact of the a/d ratio on behavior was not included in this study and is recommended for further investigation

In the first stage of the experimental program presented in Table 1, three different slag replacement levels (5%, 10%, and 15%) were investigated without fiber addition to determine the basic mechanical behavior of the geopolymer mixture. In the second stage, the slag content was fixed at 10%, which provided balanced performance in preliminary evaluations, and polyamide fiber content was added at ratios of 0%, 1%, 2%, and 3% to examine the effect of fiber reinforcement on the mechanical performance of geopolymer concrete. To evaluate the effect of curing conditions, the same mixture combinations were tested under ambient curing and oven curing, yielding a total of 12 experimental mixtures. This experimental matrix allowed for the systematic investigation of the individual effects of slag content, fiber dosage, and curing regime. After the casting process, the samples to be cured in the oven were held in a laboratory environment (±23°C) for 24 hours for initial hardening. Subsequently, the specimens were placed in a high-precision laboratory oven and exposed to a constant temperature of 85°C for 24 hours. Heating and cooling rates were controlled to prevent thermal shock and potential microcracking; after the heating cycle was completed, the specimens were allowed to cool gradually to room temperature within the oven. After the oven curing stage, the samples were stored under laboratory conditions until the 28th day of the test to ensure consistent environmental exposure.

## 3. Results and discussions

### 3.1 Beam tests

When generating the graphs, the yield point was determined using an equivalent bilinear approximation of the load–displacement curves. Accordingly, the first line was obtained based on the slope of the initial linear elastic region, and the second line was defined passing through the point corresponding to the maximum load. The intersection point of these two lines was taken as

the yield load (Py) and the corresponding yield displacement (δy). Stiffness was calculated as the slope of the linear portion in the elastic region (k=Py/δy), while the ductility ratio was determined as the ratio of the ultimate displacement to the yield displacement (μ=δu/δy).

In this study, energy absorption was calculated by integrating the area under the load-displacement curve up to a certain failure level. In theory, the load (stress)–displacement curve's enclosed area represents the fiber-reinforced composites' ability to absorb energy. Fiber reinforced concrete is typically defined by its energy absorption capacity, which is denoted by the term "toughness" [47]. The fact that the final failure point can be abrupt and irregular can create significant uncertainties in energy calculations, especially in geopolymer and cement-based composites exhibiting brittle and semi-brittle behavior. Therefore, in many studies, the load level corresponding to a certain percentage of the peak load (mostly in the 75–85% range) is accepted as the "effective failure" or "usable capacity" limit. In researchers' studies on the fracture behavior of concrete and semi-brittle materials, it has been emphasized that instabilities in the post-peak region limit the direct use of the failure point in energy-based assessments [48, 49]. Similarly, some experimental approaches proposed by [50] suggest that the area up to a certain drop rate after the peak load should be considered in energy and toughness calculations. Furthermore, According to Hewage et al. [51], the region beneath the load-displacement graph until the capacity falls to 80% of the peak value represents the residual toughness.

### 3.1.1 Evaluation of load-displacement curves under Ambient curing

Firstly, the slag ratio was changed to 5%, 10% and 15% while the amount of polyamide in the mixture was kept constant at 0%. The aim here is to observe the effect of the slag ratio on the mixture alone. While all of this was going on, the circumstances around the curing process were maintained as ambient curing. When the slag ratio is 5%, the $P_{max}$ value that is obtained from the beam is 28.47 kN, and the amount of deformation that the beam experiences is 5.15 mm. When the experiment was finished, the amount of deformation that had occurred was measured to be 5.39 mm. As a result of increasing the slag ratio to 10%, the $P_{max}$ value that was acquired from the beam was 32.19 kN, while the amount of deformation that was caused by the beam was 3.28 mm. The amount of deformation at the time of termination of the experiment was measured as 3.77 mm. Finally, when the slag ratio is raised to 15%, the $P_{max}$ value is 34.69 kN, and the beam deforms by 3.61 mm. This is the maximum value that can be achieved. At the end of the experiment, the amount of deformation was measured to be 5.40 mm. As can be seen from the test results, by increasing the slag amount from 5% to 10% and 15%, the $P_{max}$ amount carried by the beam increased by 13.07% and 21.85%. While the load-carrying capacity increased, the amount of deformation decreased by 36.31% and 29.90%. Fig. 2 displays the load-displacement diagram for various slag percentages under ambient curing conditions.

Examining the impact of raising the mixture's polyamide content by 0%, 1%, 2%, and 3% while maintaining a fixed slag ratio is another comparison under ambient curing circumstances. When the polyamide amount is 0%, the $P_{max}$ value of the beam is 32.19 kN and the deformation amount of the beam is 3.28 mm. Upon increasing the polyamide content to 1%, 2%, and 3%, the corresponding values were 35.60 kN, 36.68 kN, and 45.55 kN.The levels of deformation that correspond to these values are 1.77 mm, 4.56 mm, and 3.59 mm. As can be seen from these values, increasing the amount of polyamide in the mixture increased the load-carrying capacity of the beam. 3.03% and 27.95% are the respective rates of increase for these two parameters. The quantities of deformation that were measured are as follows: 4.69 mm, 4.97 mm, and 5.32 mm, respectively, at the moment when the experiment came at an ending. As the amount of polyamide

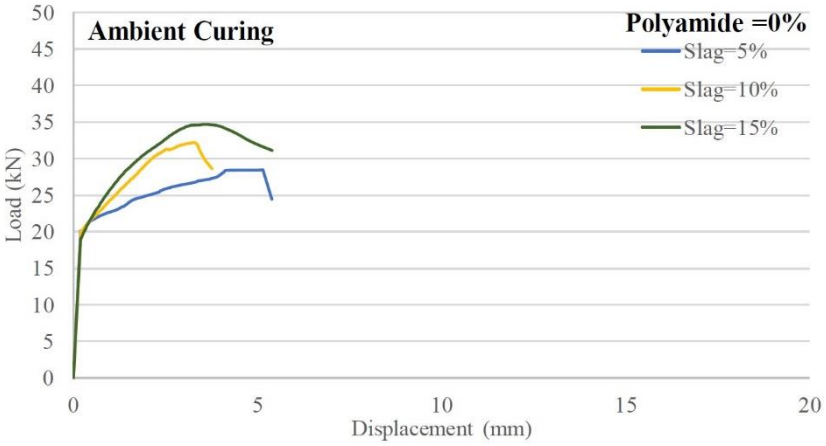



Figure 2. Under ambient curing conditions, the load-displacement diagram for a variety of slag ratios

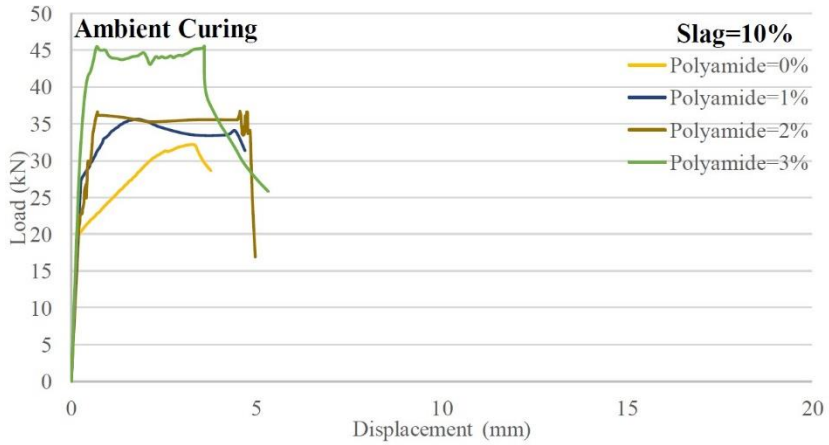



Figure 3. Under ambient curing conditions, the load-displacement diagram for a variety of Polyamide ratios

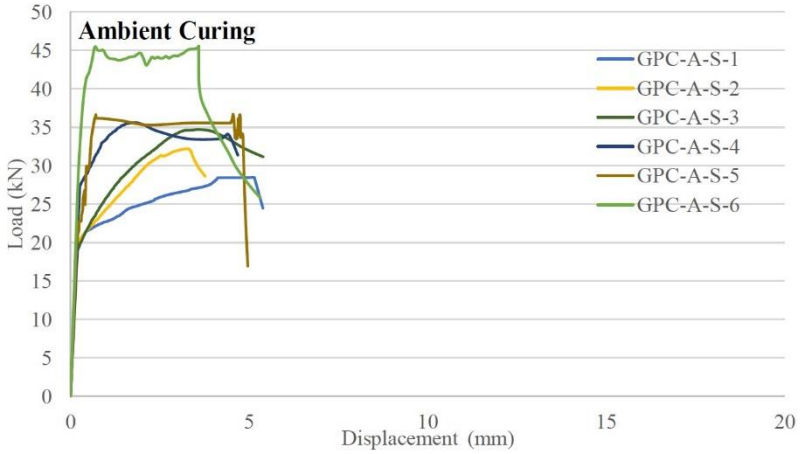



Figure 4. Under ambient curing conditions, the load-displacement diagram for a variety of all ratios

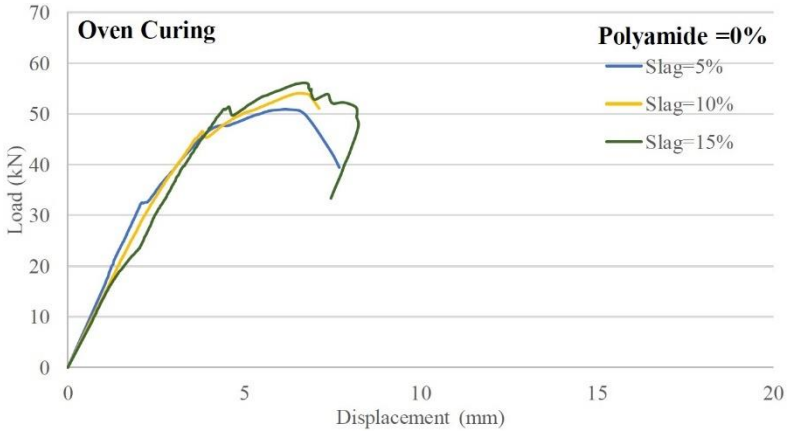



Figure 5. Under Oven curing conditions, the load-displacement diagram for a variety of slag ratios

increases, the amount of deformation of the beam also increases. For a range of polyamide ratios, Fig. 3 displays the load-displacement diagram under ambient curing conditions. Fig. 4 shows the load-displacement diagram for a range of all ratios under ambient curing conditions.

### 3.1.2 Evaluation of load-displacement curves under oven curing

Within this part, an investigation on the behavior of mixing ratios under oven curing conditions is carried out. To do this, the polyamide ratio rates were maintained at 0%, just as they were established in the preceding section. On the other hand, the slag ratio rates were altered to 5%, 10%, and 15% respectively as shown in Fig. 5. As a consequence of this modification, the $P_{max}$ load values of the beam were determined to be 50.86 kN, 54.06 kN, and 56.09 kN, respectively. The levels of deformation that correspond to these distances are 6.20 mm, 6.58 mm, and 6.70 mm. The load bearing capacity of the mixture rose by 6.29% and 10.28% when the slag ratio rates were raised by 5%, 10%, and 15% respectively. Additionally, the deformation decreased by 6.13% and 8.06% as a result of these increases. When the beam disruptions, it undergoes a maximum deformation of 7.7 mm, 7.13 mm, and 7.46 mm respectively. There is a 6.58 mm, 5.90 mm, 6.90 mm, and 9.55 mm amount of deformation that corresponds to each of these values. Subsequently, while maintaining a constant slag ratio of 0% in the mixture, the polyamide ratio was varied at 0%, 1%, 2%, and 3%. The $P_{max}$ values of the beam, on the other hand, are 54.06 kN, 56.01 kN, 56.54 kN, and 62.20 kN respectively. Increasing the Polyamide ratio from 0% to 3% caused an increase in $P_{max}$ values by 74.00%, 75.64% and 93.23%, respectively as shown in Fig. 6. When compared to this, the amount of deformation that the beam experienced increased by 79.88%, 110.37%, and 191.36% respectively. Augmenting the quantity of polyamide resulted in an enhancement of both the load-bearing capacity and the degree of distortion of the beam. Within the context of oven curing conditions, the load-displacement diagram is shown in Fig. 7 for a wide variety of ratios. Table 2 contains the data that were acquired from the evaluation of the load-displacement relationship.

These findings are comparable to those that have been discovered in previous research. When compared to samples that were cured at room temperature, samples that were cured in an oven had a strength that is somewhat greater. This is explained by the earlier polymerization that takes place during higher-temperature curing as opposed to ambient curing [52]. In addition, the link that

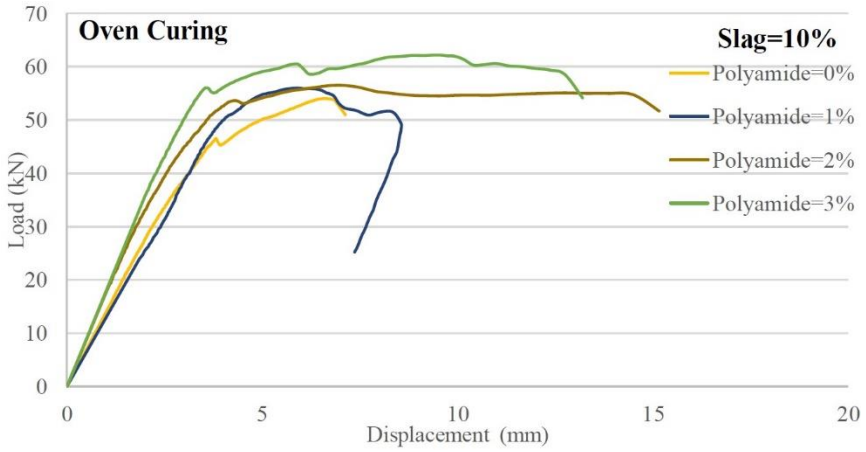



Figure 6. Under oven curing conditions, the load-displacement diagram for a variety of polyamide ratios

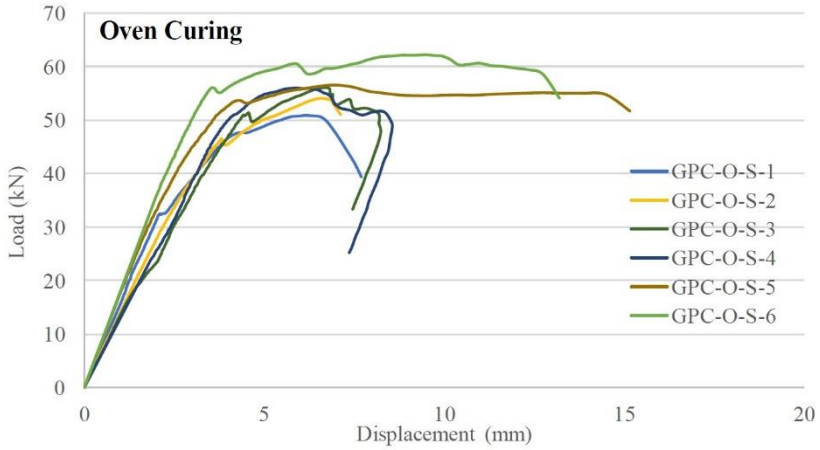



Figure 7. Under oven curing conditions, the load-displacement diagram for a variety of all ratios

forms between the gel and the aggregates, as well as the continual production of the C-A-S-H gel, are responsible for the high strength that is achieved during the oven curing process [53]. According to the findings of previous research, heat is a significant component in the process of activating fly ash. It has been claimed that in order for the reaction to take place, an activation barrier must be crossed, and that this barrier is crossed as the temperature rises [54]. According to this research, fly ash has a larger activation energy than slag, hence the heating procedure is more crucial for fly ash activation.

## 4. Evaluation of stiffness and ductility ratio

One way to describe the beam's stiffness is the load-deflection curve's slope. By using Eqs. (1) and (2), one can determine the pre-yield stiffness ($K_1$) as well as the post-yield stiffness ($K_2$). Furthermore, structures that can withstand inelastic deformation before failing without suffering a

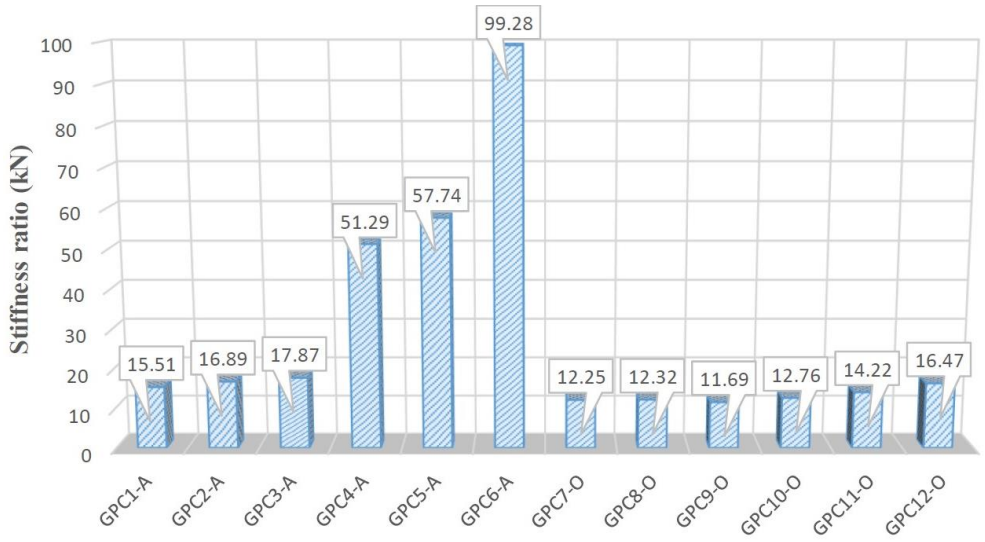



Figure 8. Under ambient and oven curing conditions, Stiffness ratio values for a variety of all mix ratios

major reduction in load-carrying capability are considered to be ductile. Several deformation-related parameters, including as joint displacement, member deviation, rotation, curvature, strain, or consumed and released energy, are often used to indicate ductility. Additionally, the ductility coefficient (μΔ) is computed using Eq. (3), as shown below. It is possible to describe the ductility of the beam as the proportion of the deflection under the yield load to the deflection under the ultimate load.

$$K_1 = {}^{P_y}\!/_{\Delta_y} \tag{1}$$

$$K_2 = {}^{P_u - P_y}\!/_{\Delta_u - \Delta_y} \tag{2}$$

$$\mu_\Delta = {}^{\Delta_u}\!/_{\Delta_y} \tag{3}$$

Pre-yield "initial" stiffness, measured in kN/mm, is denoted by the symbol $K_1$. The yielding load, $P_y$, is expressed in kN. At the yielding load, Δy is the deflection in millimeters. $K_2$ represents the "effective" stiffness after yielding, measured in kN/mm. $P_u$ represents the ultimate load measured in kN. Deformations at the ultimate load is denoted by the symbol $\Delta_u$, which is measured in millimeters. Taking into consideration the findings shown in Fig. 8 and Fig. 9, it is possible to conclude that the bending stiffness increase in proportion to the slag ratio. In contrast, it has been shown that the stiffness ratio decreases significantly in proportion to the rise in the polyamide ratio. When compared to ambient curing, it has been discovered that the stiffness ratio shows a modest drop when the material is cured in an oven. An increase in stiffness can be observed with a higher slag ratio. An increase in the polyamide ratio was found to result in a reduction in the stiffness of the material when it was cured in an oven.

A noticeable rise in the ductility ratio was seen in the case of ambient curing, particularly in conjunction with the rise in the polyamide ratio. On the other hand, while there was a discernible

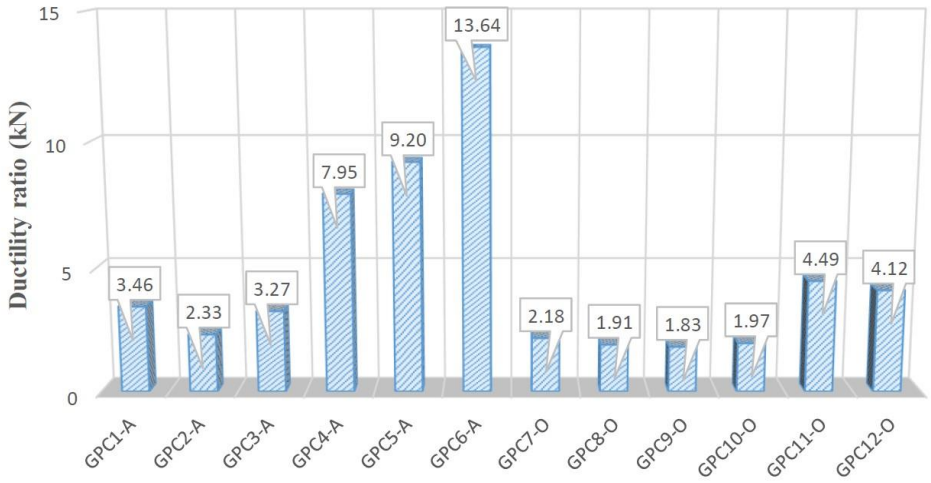



Figure 9. Under ambient and oven curing conditions, ductility ratio values for a variety of all mix ratios

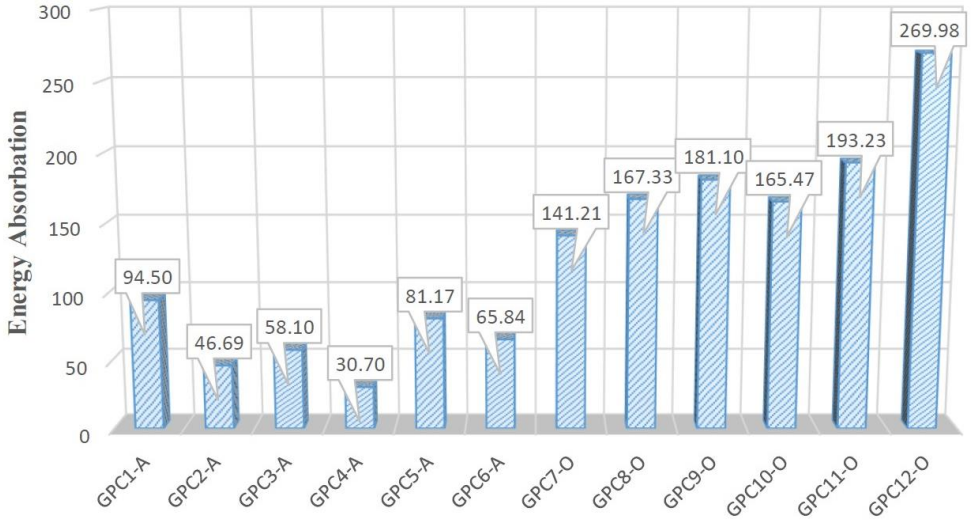



Figure 10. Under ambient and oven curing conditions, energy absorbation values for a variety of all mix ratios

decline in the ductility ratio in the oven curing scenario, particularly with the improvement in the slag ratio, there was a modest improvement detected with the incorporation of the polyamide ratio into the mixture. For the purpose of calculating the energy ductility, which is shown in Fig. 10, it was assumed that the failure point is achieved when the applied load reduces to 80% of its maximum value. When the amount of slag ratio reinforcement was increased during ambient curing, it was noticed that both the energy absorption capacity and the ultimate load decreased. This is demonstrated in Fig. 10, which indicates that this phenomenon occurred. Additionally, it has been found that the additional polyamide ratio results in an approximately two-fold increase in energy absorption capacity in ambient curing. When compared to GPC1-A, GPC2-A and GPC3-A, the energy absorption capacity of GPC7-O, GPC8-O and GPC9-O shown a significant increase

Table 2. Values obtained from the load-displacement

| | Test no | $P_{Max}$ (kN) | Def. at the $P_{Max}$ (mm) | $\delta_u$ (mm) | Stifness at $P_{max}$ (kN/mm) | $P_u$ ($0.85P_{max}$) (kN) | Displacement at Yield $\delta_y$ (mm) | Stiffness at Yield (kN/mm) | Ductility ratio |
|---|---|---|---|---|---|---|---|---|---|
| Ambinet | GPC1-A | 28.47 | 5.15 | 5.39 | 5.53 | 24.20 | 1.56 | 15.51 | 3.46 |
| | GPC2-A | 32.19 | 3.28 | 3.77 | 9.81 | 27.36 | 1.62 | 16.89 | 2.33 |
| | GPC3-A | 34.69 | 3.61 | 5.4 | 9.61 | 29.49 | 1.65 | 17.87 | 3.27 |
| | GPC4-A | 35.6 | 1.77 | 4.69 | 20.11 | 30.26 | 0.59 | 51.29 | 7.95 |
| | GPC5-A | 36.68 | 4.56 | 4.97 | 8.04 | 31.18 | 0.54 | 57.74 | 9.20 |
| | GPC6-A | 45.55 | 3.59 | 5.32 | 12.69 | 38.72 | 0.37 | 99.28 | 13.64 |
| Oven | GPC7-O | 50.86 | 6.2 | 7.7 | 8.20 | 43.23 | 3.53 | 12.25 | 2.18 |
| | GPC8-O | 54.06 | 6.58 | 7.13 | 8.22 | 45.95 | 3.73 | 12.32 | 1.91 |
| | GPC9-O | 56.09 | 6.7 | 7.46 | 8.37 | 47.68 | 4.08 | 11.69 | 1.83 |
| | GPC10-O | 56.01 | 5.9 | 7.36 | 9.49 | 47.61 | 3.73 | 12.76 | 1.97 |
| | GPC11-O | 56.54 | 6.9 | 15.16 | 8.19 | 48.06 | 3.38 | 14.22 | 4.49 |
| | GPC12-O | 62.2 | 9.55 | 13.21 | 6.51 | 52.87 | 3.21 | 16.47 | 4.12 |

of around 49.42%, 258.38% and 211.69%, respectively. When comparing GPC4-A, GPC5-A and GPC6-A to GPC10-O, GPC11-O and GPC12-O, the energy absorption capacity increased by approximately 438.96%, 138.07% and 310.05%.

## 5. Evaluation of beam failure modes and cracks

The presence of shear fractures in reinforced concrete beams is a typical and inevitable characteristic. As shown in Fig. 11, beginning at the tension face, the shear fractures spread in a direction that was perpendicular to the axis of the member from which they originated. Factors include the tensile stress in the longitudinal bars, the extent of the concrete cover, the dimension and distance of the longitudinal bars, the beam profundity, the neutral axis position, bond strength, and the concrete's tensile strength, which all affect how wide a shear fracture is. There is a diagonal extension of the tensile cracks towards the loads and supports, as indicated in Fig. 11, when the applied load is increased. It was determined that the shear crack angles were calculated by taking the average angle of each main crack. One might draw the conclusion that the shear crack angles change along the shear span based on what is visible in the figures. These shear fractures, which are located close to the stress point, exhibit a more acute shear fracture slope. Advancing closer to the location of support causes these angles to begin to lower. The first set of ruptures consisted of flexural fractures that appeared in the mid-span zone. Gradually, as the load rose, a series of flexural fractures appeared in the shear span location. Following that, it turned to create flexural-shear fractures that connected the loading and supporting locations, and further shear fractures occurred during the successive loading stages. There were considerable and broader fractures in the shear fracture region as a consequence of the shear failure mode. Beginning with the initial fracture and continuing until failure, there are two phases: the stable fracturing period, during which only shear fractures are expected to widen, and the fracture creation phase, during which new shear fractures appear. An increase in the shear loads in RC cracked elements was



Figure 11. A representative example of a shear fracture obtained during testing

shown to result in a considerable deformation of the concrete between the shear fractures, which in turn led to a reduction in the diagonal fracture distance at the points of fracture.

When the ratio of slag in the mixture is increased, it has been noticed that the cracks that tend to appear in the mixture become less frequent. A further observation was made that the beam had a lower degree of dispersion. A discernible reduction in the number of cracks as well as their breadth was seen as a result of increasing the quantity of polyamide present in the mixture. The simultaneous increase in both load-carrying capacity and deformation capability observed with an increase in fiber content varies depending on the multi-stage energy dissipation mechanisms within the composite matrix. During the formation of microcracks, the fibers randomly distributed throughout the matrix act as crack bridges, transferring stress from the crack tip to sound regions. In this process, the high ductility of the polyamide fibers and their interfacial bond with the matrix allow the fibers to absorb a large amount of mechanical energy through fiber slippage or controlled fiber breakage rather than sudden brittle fracture. Consequently, the increased fiber volume stabilizes crack propagation and enhances the material's ductility, while the friction resistance at the fiber-matrix interface also increases the composite's ultimate load-bearing capacity. Furthermore, when it comes to polymer fibers, the force values that are measured are influenced by the elongation of the fiber as well as the plastic deformation of the surface of the fiber [55]. In the frictional sliding zone of the pullout, the pullout force increases as the embedded length increases, which is because the fiber abrasion effect becomes more noticeable as the length of the fibers increases. Because of their better tensile strength and stiffness, synthetic fibers greatly increase the ductility of concrete [56]. When confronted with flexural stresses, these fibers are essential in preventing sudden, brittle failure and impeding the propagation of cracks. Synthetic fibers slowly reduce load-bearing capacity after peak load by bridging fractures and transferring loads across the fracture plane, enhancing post-peak performance [57]. After micro-cracks form, synthetic fibers bridge them to distribute stress and prevent rapid crack spreading [58]. Strengthening their mechanical contact with the concrete matrix improves stress transmission, increasing energy absorption and structural integrity even under harsh situations [59]. Synthetic fibers may deflect and hinder fractures, forcing them to circumnavigate them rather than spread through them [60]. By increasing crack propagation energy, this deflection mechanism improves concrete fracture toughness and durability [61].

Upon examining the post-fracture crack patterns of the specimens (Fig. 11), it was determined that the plastic fiber content and the curing regimen applied had a significant effect on crack morphology. While single, brittle macro-cracks with an average width of 1.8 mm and oriented parallel to the load direction (0°-15°) were observed in the control specimens (Ambient-0% Plastic), this structure transformed into a multi-capillary crack form with fiber reinforcement. In particular, in the Oven-20% Plastic group, it was determined that the crack spacing fell within the 10-18 mm range and the average crack width decreased to as low as 0.3 mm. This demonstrates that the plastic fibers, homogeneously distributed within the matrix, successfully transfer stress from the crack tip to sound regions via the crack-bridging mechanism and disperse energy over a wider area. Additionally, the fact that the crack angles in the oven-cured specimens deviate from the load direction to reach levels of 45°-60° is a structural indicator of increased ductility and energy absorption capacity of the material.

This experiment's goal is to demonstrate the beam's shear behavior in relation to the chosen design and reinforcement configuration. Flexural cracks may develop under loading, nevertheless, since the reinforcement ratio also affects the beams' flexural stiffness and fracture distribution. Slag inclusion and polyamide fibers under oven-curing conditions improve fracture-bridging and matrix integrity, which promotes shear load-transfer mechanisms and slows diagonal shear crack growth [62, 63].

## 6. Evaluation of test results with design codes

To make a prediction regarding the ultimate shear capacity of the beams that were tested, this section makes use of four well-known design codes and equations that have been suggested. ACI 318-14 [64] and CEB-FIB [65] were the design codes that were utilized. Eq. (4) and Equation (5) respectively present the codes. Furthermore, the following formulas (Eq. (6) and Eq. (7)) are included in the Iranian national building codes and Eurocode for calculating the nominal shear stress and strength: To accurately predict the power of the test beam, it is crucial to consider each of these factors. In MPa, $f_c$ stands for the cylinder's CS.The width of the beam, measured in millimeters, is denoted by the letter b. The beam's effective depth, denoted by d, is measured in millimeters. Concrete's coefficient of safety is ϕ, with a value of 0.60.

$$V_C = 0.15\left(1+\sqrt{200/d}\right)\left(3\frac{d}{a}\right)^{1/3}(100.\rho f_c')^{1/3}b_w d \tag{4}$$

$$V_{pred} = 0.17.\lambda(f_c')^{1/2}b_w d \tag{5}$$

$$V_C = 0.2.\phi.\left(\sqrt{f_c'}\right)b_w d \tag{6}$$

$$V_C = 0.18.(1+\sqrt{200/d}.\left(100.\rho\sqrt{f_c'}\right)^{1/3} \tag{7}$$

To evaluate the predictive capability of design standards, the ratios between experimental data and theoretical calculations ($P_{exp}/P_{pred}$) were systematically analyzed. The results of these calculations showed that the ACI 318 and Eurocode 2 standards yielded average ratios of 1.15 and 1.22, respectively, for samples containing polyamide fibers. The fact that these ratios exceed 1.0

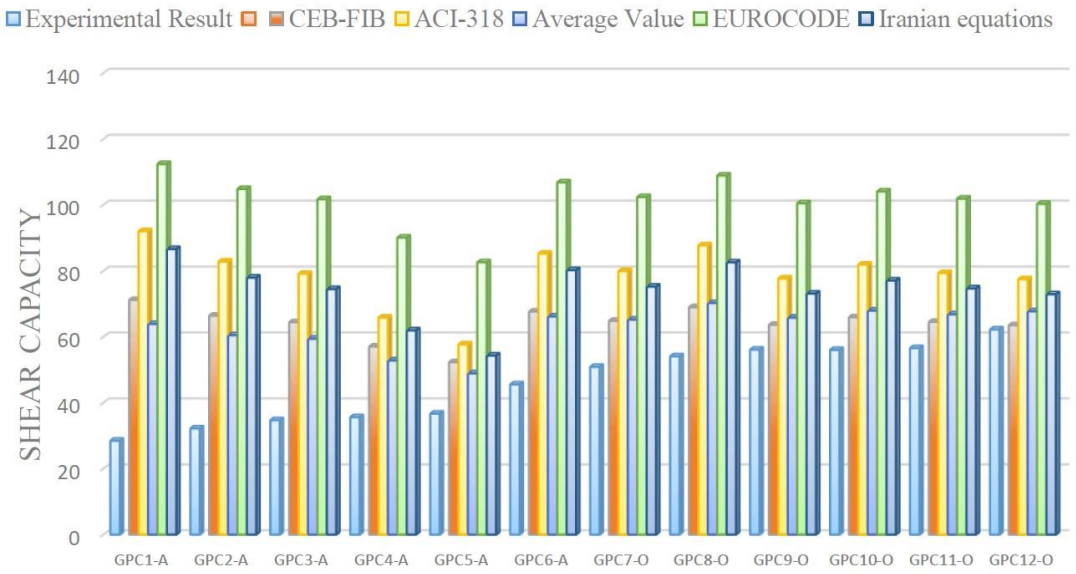



Figure 12. Various design regulations and recommended shear capacity equations

demonstrates that the current standards provide conservative predictions for such innovative concrete components and remain on the safe side. However, the increase in standard deviation and coefficient of variation (COV) in specimens with 20% polyamide content indicates that the current formulations deviate from the assumption of homogeneity at high fiber ratios. The comparison graph presented in Fig. 12 reveals that the CEB-FIB model provides the closest prediction to experimental results (MAPE: 8.4%), but has the lowest safety margin.

## 7. Conclusions

The purpose of this research was to investigate the shear behavior and fracture behavior of various RCBs via the use of experimental experimentation. The goal was to ascertain how the reinforced geopolymer concrete was impacted by the slag proportion, polypropylene fiber concentrations, and curing procedures. A total of four essential parameters were taken into consideration during the production of the specimens. These parameters were the proportion of slag, the presence of polypropylene fiber, the method of ambient curing, and the method of oven curing. Changing the slag ratios to 0%, 5%, 10%, and 15% was the means by which this objective was accomplished. Additionally, the percentages that were selected for the fibers that were created from polypropylene were 1%, 2%, and 3%. After being prepared in the lab, RCBs undergo a thorough inspection for fractures and bending behaviors that align with the outcomes of the experimental testing. These important facts are evaluated in the study that follows:

- The influence of the slag ratio was investigated while the polypropylene fiber ratio was held constant throughout the experiment. Based on the findings, it was discovered that an increase in the slag ratio had a direct influence on the load bearing capabilities of R-C-Bs. The load bearing capacity of R-C-B was enhanced by 21.85% as a consequence of the 15% rise in the slag ratio that occurred throughout the process of ambient curing. It was

determined that the load bearing capacity of R-C-B was increased by 10.28% as a result of the 15% improvement in the slag percentage that occurred throughout the oven curing process. Comparative studies have shown that increasing the slag ratio during oven curing has a positive effect on the load carrying ability of R-C-B compared to ambient temperature curing.

- It is widely accepted that the ratio of polypropylene fibers significantly influences the fracture behavior of R-C-Bs. R-C-B's load-carrying capacity was improved by 25.04% when the polypropylene fibers ratio was increased by 1% during the ambient curing process. Additionally, there was a reduction in deformation capacity to be about 12.98%. When the polyamide ratio was increased by 1% during the over-curing process, the R-C-B's load-carrying capacity rose by 10.12%. This was a significant performance improvement. Additionally, there was a considerable drop in the capacity for deformation, which was 4.41%.
- As a result of a comparison of the impacts of ambient curing and oven curing on the polyamide ratio and slag ratio, it was discovered that the oven curing technique has a bigger influence on load-bearing capacity than the ambient curing approach does. This is due to the fact that polymerization occurs prematurely during higher-temperature curing, as opposed to ambient curing.
- Comparing the design codes reveals that the CEB-FIB equation yields the closest results when using Oven curing. In this case, GPC12-O provided the closest result, yielding an approximate value of 2.10%.
- Slag addition increases matrix densification and interfacial bonding, increasing load-bearing capability under ambient and oven curing conditions. From the standpoint of structural design, this implies that slag-based combinations might enhance load-carrying parts' mechanical dependability while simultaneously promoting sustainability by lowering cement use.
- Due to crack-bridging and stress redistribution, polypropylene and polyamide fibers increased load-carrying ability. Due of the decrease in deformation ability, high fiber content may stiffen and restrict ductility. Fiber dose adjustment is needed to balance strength and deformability in structural applications.
- Geopolymerization and matrix formation increase with oven curing, hence it yielded larger strength improvements than ambient curing. For precast structural elements needing strong early-age strength, oven curing may be preferred, but ambient curing may be better for cast-in-place applications due to realistic construction circumstances and energy economy.

## Acknowledgments

This study was supported by the grant of the Russian Science Foundation No. 25-79-32007, https://rscf.ru/project/25-79-32007/.

## References

1. Ramujee, K., PothaRaju, M. (2017). Mechanical properties of geopolymer concrete composites. Materials Today: Proceedings, 4(2), 2937-2945. https://doi.org/10.1016/j.matpr.2017.02.175.

2. Pavithra, P., Reddy, M.S., Dinakar, P., Rao, B.H., Satpathy, B.K., Mohanty, A.N. (2016). A mix design procedure for geopolymer concrete with fly ash. Journal of Cleaner Production, 133, 117-125. https://doi.org/10.1016/j.jclepro.2016.05.041.
3. Hassan, A., Arif, M., Shariq, M. (2019). Influence of microstructure of geopolymer concrete on its mechanical properties—a review. Advances in Sustainable Construction Materials and Geotechnical Engineering: Select Proceedings of TRACE 2018, 119-129. https://doi.org/10.1007/978-981-13-7480-7_10.
4. Zhuang, X.Y., Chen, L., Komarneni, S., Zhou, C.H., Tong, D.S., Yang, H.M., ... Wang, H. (2016). Fly ash-based geopolymer: clean production, properties and applications. Journal of Cleaner Production, 125, 253-267. https://doi.org/10.1016/j.jclepro.2016.03.019.
5. Kim, J.S., Park, J. (2014). An experimental evaluation of development length of reinforcements embedded in geopolymer concrete. Applied Mechanics and Materials, 578, 441-444. https://doi.org/10.4028/www.scientific.net/AMM.578-579.441.
6. Turk, J., Cotič, Z., Mladenovič, A., Šajna, A. (2015). Environmental evaluation of green concretes versus conventional concrete by means of LCA. Waste Management, 45, 194-205. https://doi.org/10.1016/j.wasman.2015.06.035.
7. Malkawi, A.B., Nuruddin, M.F., Fauzi, A., Almattarneh, H., Mohammed, B.S. (2016). Effects of alkaline solution on properties of the HCFA geopolymer mortars. Procedia Engineering, 148, 710-717. https://doi.org/10.1016/j.proeng.2016.06.581.
8. Nath, P., Sarker, P.K., Rangan, V.B. (2015). Early age properties of low-calcium fly ash geopolymer concrete suitable for ambient curing. Procedia Engineering, 125, 601-607. https://doi.org/10.1016/j.proeng.2015.11.077.
9. Saxena, S.K., Kumar, M., Singh, N.B. (2017). Fire resistant properties of alumino silicate geopolymer cement mortars. Materials Today: Proceedings, 4(4), 5605-5612. https://doi.org/10.1016/j.matpr.2017.06.018.
10. Nath, P., Sarker, P.K. (2017). Flexural strength and elastic modulus of ambient-cured blended low-calcium fly ash geopolymer concrete. Construction and Building Materials, 130, 22-31. https://doi.org/10.1016/j.conbuildmat.2016.11.034.
11. Kong, D.L., Sanjayan, J.G. (2010). Effect of elevated temperatures on geopolymer paste, mortar and concrete. Cement and Concrete Research, 40(2), 334-339. https://doi.org/10.1016/j.cemconres.2009.10.017.
12. Kong, D.L., Sanjayan, J.G., Sagoe-Crentsil, K. (2007). Comparative performance of geopolymers made with metakaolin and fly ash after exposure to elevated temperatures. Cement and Concrete Research, 37(12), 1583-1589. https://doi.org/10.1016/j.cemconres.2007.08.021.
13. Assi, L., Ghahari, S., Deaver, E.E., Leaphart, D., Ziehl, P. (2016). Improvement of the early and final compressive strength of fly ash-based geopolymer concrete at ambient conditions. Construction and Building Materials, 123, 806-813. https://doi.org/10.1016/j.conbuildmat.2016.07.069.
14. Lokuge, W., Wilson, A., Gunasekara, C., Law, D.W., Setunge, S. (2018). Design of fly ash geopolymer concrete mix proportions using Multivariate Adaptive Regression Spline model. Construction and Building Materials, 166, 472-481. https://doi.org/10.1016/j.conbuildmat.2018.01.175.
15. Hassan, A., Arif, M., Shariq, M. (2019). Effect of curing condition on the mechanical properties of fly ash-based geopolymer concrete. SN Applied Sciences, 1(12), 1694. https://doi.org/10.1007/s42452-019-1774-8.
16. Hassan, A., Arif, M., Shariq, M. (2020). Mechanical behaviour and microstructural investigation of geopolymer concrete after exposure to elevated temperatures. Arabian Journal for Science and Engineering, 45(5), 3843-3861. https://doi.org/10.1007/s13369-019-04269-9.
17. Vijai, K., Kumutha, R., Vishnuram, B.G. (2010). Effect of types of curing on strength of geopolymer concrete. International Journal of the Physical Sciences, 5(9), 1419-1423.
18. Nath, P., Sarker, P.K. (2014). Effect of GGBFS on setting, workability and early strength properties of fly ash geopolymer concrete cured in ambient condition. Construction and Building materials, 66, 163-171. https://doi.org/10.1016/j.conbuildmat.2014.05.080.

19. Gupta, T., Saraswat, V., Meesala, C.R. (2024). Effect of recycled aggregate on properties of blended geopolymer concrete cured at ambient temperature. Advances in Concrete Construction, 18(3), 191-204. https://doi.org/10.12989/acc.2024.18.3.191.
20. Zafar, I., Tahir, M.A., Hameed, R., Rashid, K., Ju, M. (2022). Reactivity of aluminosilicate materials and synthesis of geopolymer mortar under ambient and hot curing condition. Advances in Concrete Construction, 13(1), 71-81. https://doi.org/10.12989/acc.2022.13.1.071.
21. Esparham, A., Moradikhou, A.B., Andalib, F.K., Avanaki, M.J. (2021). Strength characteristics of granulated ground blast furnace slag-based geopolymer concrete. Advances in Concrete Construction, 11(3), 219-229. https://doi.org/10.12989/acc.2021.11.3.219.
22. Perera, D.S., Uchida, O., Vance, E.R., Finnie, K.S. (2007). Influence of curing schedule on the integrity of geopolymers. Journal of Materials Science, 42(9), 3099-3106. https://doi.org/10.1007/s10853-006-0533-6.
23. Heah, C.Y., Kamarudin, H., Al Bakri, A.M., Binhussain, M., Luqman, M., Nizar, I.K., ... Liew, Y.M. (2011). Effect of curing profile on kaolin-based geopolymers. Physics Procedia, 22, 305-311. https://doi.org/10.1016/j.phpro.2011.11.048.
24. Rovnaník, P. (2010). Effect of curing temperature on the development of hard structure of metakaolin-based geopolymer. Construction and Building Materials, 24(7), 1176-1183. https://doi.org/10.1016/j.conbuildmat.2009.12.023.
25. Shoaei, P., Momenzadeh, A., Hosseini, H., Rajaei, S., Ameri, F., Pilehvar, S. (2024). One-part slag/zeolite geopolymer mortars under ambient and heat curing conditions. Case Studies in Construction Materials, 20, e02677. https://doi.org/10.1016/j.cscm.2023.e02677.
26. Wang, C., Zhao, L., Guo, Z., Hou, C., Yao, S., Zhang, F., ... Zhang, H. (2024). Mechanistic study of fly ash activity enhanced by high temperature to strengthen cementitious materials. Construction and Building Materials, 416, 135026. https://doi.org/10.1016/j.conbuildmat.2024.135026.
27. Zheng, J., Li, X., Bai, C., Zheng, K., Wang, X., Sun, G., ... Colombo, P. (2024). Rapid fabrication of porous metakaolin-based geopolymer via microwave foaming. Applied Clay Science, 249, 107238. https://doi.org/10.1016/j.clay.2023.107238.
28. Yewale, V.V., Shirsath, M.N., Hake, S.L. (2016). Evaluation of efficient type of curing for geopolymer concrete. Evaluation, 3(8), 10-14.
29. Kumaravel, S. (2014). Development of various curing effect of nominal strength Geopolymer concrete. Journal of Engineering Science and Technology Review, 7(1), 116-119.
30. Zhang, Z., Provis, J.L., Reid, A., Wang, H. (2014). Geopolymer foam concrete: an emerging material for sustainable construction. Construction and Building Materials, 56, 113-127. https://doi.org/10.1016/j.conbuildmat.2014.01.081.
31. Mo, K.H., Yeap, K.W., Alengaram, U.J., Jumaat, M.Z., Bashar, I.I. (2018). Bond strength evaluation of palm oil fuel ash-based geopolymer normal weight and lightweight concretes with steel reinforcement. Journal of Adhesion Science and Technology, 32(1), 19-35. https://doi.org/10.1080/01694243.2017.1336195.
32. Habert, G., De Lacaillerie, J.D.E., Roussel, N. (2011). An environmental evaluation of geopolymer based concrete production: reviewing current research trends. Journal of Cleaner Production, 19(11), 1229-1238. https://doi.org/10.1016/j.jclepro.2011.03.012.
33. Çelikten, S. (2022). Properties of recycled steel fibre reinforced expanded perlite based geopolymer mortars. Advances in Concrete Construction, 13(1), 25-34. https://doi.org/10.12989/acc.2022.13.1.025.
34. Mohamed, A.Y., Canpolat, O., Al-Mashhadani, M.M. (2022). Mechanical and durability of geopolymer concrete containing fibers and recycled aggregate. Computers and Concrete, 30(6), 421. https://doi.org/10.12989/cac.2022.30.6.421.
35. Yilmazoglu, A., Yıldırım, S.A.L.İ.H., Genc, M. (2024). Multi-response optimization of FA/GGBS-based geopolymer concrete containing waste rubber fiber using Taguchi-Grey relational analysis. Computers and Concrete, 34(2), 213. https://doi.org/10.12989/cac.2024.34.2.213.
36. Celik, A.I., Özkiliç, Y.O. (2024). Lightweight geopolymer concrete using pumice and glass fiber. Computers and Concrete, 34(5), 577. https://doi.org/10.12989/cac.2024.34.5.577.

37. Çelik, A.L.I., Ozkilic, Y. (2023). Geopolymer concrete with high strength, workability and setting time using recycled steel wires and basalt powder. Steel and Composite Structures, 46(5), 689-707. https://doi.org/10.12989/scs.2023.46.5.689.
38. Bernal, S., De Gutierrez, R., Delvasto, S., Rodriguez, E. (2010). Performance of an alkali-activated slag concrete reinforced with steel fibers. Construction and Building Materials, 24(2), 208-214. https://doi.org/10.1016/j.conbuildmat.2007.10.027.
39. Hassan, A., Arif, M., Shariq, M. (2021). Structural performance of ambient-cured reinforced geopolymer concrete beams with steel fibres. Structural Concrete, 22(1), 457-475. https://doi.org/10.1002/suco.202000191.
40. Sumajouw, M.D.J., Rangan, B.V. (2006). Low-calcium fly ash-based geopolymer concrete: reinforced beams and columns. Curtin University of Technology.
41. Ferdous, W., Manalo, A., Khennane, A., Kayali, O. (2015). Geopolymer concrete-filled pultruded composite beams–concrete mix design and application. Cement and Concrete Composites, 58, 1-13. https://doi.org/10.1016/j.cemconcomp.2014.12.012.
42. Kumaravel, S., Thirugnanasambandam, S. (2013). Flexural behaviour of reinforced low calcium fly ash based geopolymer concrete beam. Global Journals of Research in Engineering, 13(8), 9.
43. Hutagi, A., Khadiranaikar, R.B. (2016). Flexural behavior of reinforced geopolymer concrete beams. 2016 international conference on electrical, electronics, and optimization techniques (ICEEOT), 3463-3467. https://doi.org/10.1109/ICEEOT.2016.7755347.
44. Abdullah, M., Qazi, A.U., Khan, Q.S., Kazmi, S.M.S., Munir, M.J. (2024). Experimental and analytical investigations on shear performance of Ambient-Cured reinforced geopolymer concrete beams. Buildings, 14(1), 204. https://doi.org/10.3390/buildings14010204.
45. Çelik, A.İ., Tunç, U., Karalar, M., Guven, A., Ozkilic, Y.O. (2025). Bending behavior of reinforced geopolymer concrete beams with varying proportions of slag and polyamide fibers in oven and ambient curing. Advances in Concrete Construction, 20(6), 469-481. https://doi.org/10.12989/acc.2025.20.6.469.
46. ASCE-ACI Committee 445 on Shear and Torsion (1998). Recent approaches to shear design of structural concrete. Journal of Structural Engineering, 124(12), 1375-1417.
47. Christopher, C.G., Gopal, R., Sadasivam, S., Devi Keerthika Esakki, A.K., Dinesh Kumar, P. (2023). Experimental toughness and durability evaluation of FRC composite reinforced with steel–polyester fiber combination. International Journal of Concrete Structures and Materials, 17(1), 39. https://doi.org/10.1186/s40069-023-00599-z.
48. DiTommaso, A. (1984). Evaluation of concrete fracture. Fracture mechanics of concrete: material characterization and testing, Springer Netherlands, Dordrecht.
49. Shah, S.P., Swartz, S.E., Ouyang, C. (1995). Fracture mechanics of concrete: applications of fracture mechanics to concrete, rock and other quasi-brittle materials. John Wiley & Sons.
50. Rilem, D.R. (1985). Determination of the fracture energy of mortar and concrete by means of three-point bend tests on notched beams. Materials and Structures, 18(106), 285-290.
51. Hewage, D.K., Camille, C., Mirza, O., Mashiri, F., Kirkland, B., Clarke, T. (2024). Effect of post-peak flexural toughness on the residual performance of macro synthetic fibre reinforced concrete sleepers subjected to impact loading. Engineering Structures, 307, 117913. https://doi.org/10.1016/j.engstruct.2024.117913.
52. Poloju, K.K., Srinivasu, K. (2021). Impact of GGBS and strength ratio on mechanical properties of geopolymer concrete under ambient curing and oven curing. Materials Today: Proceedings, 42, 962-968. https://doi.org/10.1016/j.matpr.2020.11.934.
53. Goriparthi, M.R., TD, G.R. (2017). Effect of fly ash and GGBS combination on mechanical and durability properties of GPC. Advances in Concrete Construction, 5(4), 313. https://doi.org/10.12989/acc.2017.5.4.313.
54. Hou, Y., Wang, D., Zhou, W., Lu, H., Wang, L. (2009). Effect of activator and curing mode on fly ash-based geopolymers. Journal of Wuhan University of Technology-Material Science Edition, 24(5), 711-715. https://doi.org/10.1007/s11595-009-5711-3.
55. Wölfel, E., Brünig, H., Curosu, I., Mechtcherine, V., Scheffler, C. (2021). Dynamic single-fiber pull-out

of polypropylene fibers produced with different mechanical and surface properties for concrete reinforcement. Materials, 14(4), 722. https://doi.org/10.3390/ma14040722.

56. Alabdulkarim, A., El-Sayed, A.K., Alsaif, A.S., Fares, G., Alhozaimy, A.M. (2024). Behavior of lightweight self-compacting concrete with recycled tire steel fibers. Buildings, 14(8), 2463. https://doi.org/ 10.3390/buildings14082463.
57. Akbulut, Z.F., Tawfik, T.A., Smarzewski, P., Guler, S. (2025). Advancing hybrid fiber-reinforced concrete: performance, crack resistance mechanism, and future innovations. Buildings, 15(8), 1247. https://doi.org/10.3390/buildings15081247.
58. Zahid, M., Khan, M.I., Shafiq, N., Abbas, Y.M., Khatib, J.M. (2024). Achieving superior mechanical performance in one-part geopolymer composites through innovative hybrid fiber systems of recycled steel and PVA fibers. Journal of Materials Research and Technology, 32, 1772-1787. https://doi.org/10.1016/j.jmrt.2024.08.002.
59. Li, L., Shu, W., Xu, H., Rui, X., Wang, Z., Zeng, Y., ... Zhu, Z. (2024). Experimental study on flexural toughness of fiber reinforced concrete beams: effects of cellulose, polyvinyl alcohol and polyolefin fibers. Journal of Building Engineering, 81, 108144. https://doi.org/10.1016/j.jobe.2023.108144.
60. Jiang, Y., Yan, Y., Li, T., Cao, X., Yu, L., Qi, H. (2023). Comparison of the mechanical properties and crack expansion mechanism of different content and shapes of brass-coated steel fiber-reinforced ultra-high-performance concrete. Materials, 16(6), 2257. https://doi.org/10.3390/ma16062257.
61. Syduzzaman, M., Rumi, S.S., Fahmi, F.F., Akter, M., Dina, R.B. (2023). Mapping the recent advancements in bast fiber reinforced biocomposites: a review on fiber modifications, mechanical properties, and their applications. Results in Materials, 20, 100448. https://doi.org/10.1016/j.rinma.2023.100448.
62. Ahmed, T., Chidambaram, R. S. (2022). Shear strength of steel fiber reinforced concrete beam–a review. Materials Today: Proceedings, 64, 1087-1093. https://doi.org/10.1016/j.matpr.2022.05.368.
63. Al-Khafaji, N.H., Harba, I.S. (2023). Shear and flexural behavior of lightweight concrete beams containing hybrid fibers. Civil and Environmental Engineering, 19(1), 206-217. https://doi.org/10.2478/cee-2023-0018.
64. 318R-14 A. (2014). A.C.I. committee 318, building code requirements for structural concrete and commentary. Farmington Hills, 524.
65. CEB-FIP (1993). CEB-FIP, CEB-FIP model code for concrete structures. Comite Euro-International du Beton, Federation International de la Precontrainte.